

Electron Energy Characteristics of Two-Dimensional Hydroxysiloxane Structures with Defects of Substitution of Silicon Atoms by Titanium and Zirconium Atoms

Nguyen Thi Sa,

Doctor of Philosophy (Ph. D.), Lecturer

Hanoi University of Industry, Faculty of Fundamental Sciences, Department of Physics.

E-mail: nguyenthisa@hau.edu.vn

Trinh Thi Thu Huong,

Master of Science (M. Sc.), Lecturer

Hanoi University of Industry, Department of Science and Technology.

E-mail: trinthithuhuong@hau.edu.vn

Article Info

Page Number: 103 - 111

Publication Issue:

Vol 71 No. 3 (2022)

Abstract

A computation scheme based on density functional theory adapted for structures with translational symmetry with full optimization of geometrical parameters is applied to calculate the two-dimensional dielectric (single layer) hydroxysiloxane structures as an ideal composition as well as with defects of substitution of silicon atoms by titanium and zirconium atoms. The dependence of the electron energy spectrum and position of the optical absorption curves both on the type of atoms-substituents and their concentration is investigated. It is shown that at the substitution, besides boundaries shifts of energy bands and their widths, states with energies inside the region of forbidden energies corresponding to defect-free structure occur. Optical transitions involving these states appear in the absorption spectrum or in the form of separated bands, or of bands merging with the ones corresponding to transitions from 2p-top of valence band into the conduction band in dependence on the type of substituting atoms.

Keywords: DFT calculations, two-dimensional silica, substitution defect.

Article History

Article Received: 12 January 2022

Revised: 25 February 2022

Accepted: 20 April 2022

Publication: 27 May 2022

1. Introduction

Low-dimensional semiconductor and dielectric materials have attracted the attention of many researchers due to the possibility of manifestation of new physical effects that are absent for the bulk phase of compounds of the same composition. These effects play an important role in the selection of materials for micro- and nanoelectronic technology [1–4]. Such objects include, in particular, two-dimensional hydroxysiloxane (2D HS) structures, which can be imagined as a finite number of layers isolated from crystalline modifications of silicon dioxide (β -cristobalite or β -tridymite) with the closure of broken valences (Si–O bonds perpendicular to the layer surface) by hydrogen atoms (with the formation of a surface hydroxide cover) (Fig. 1a).

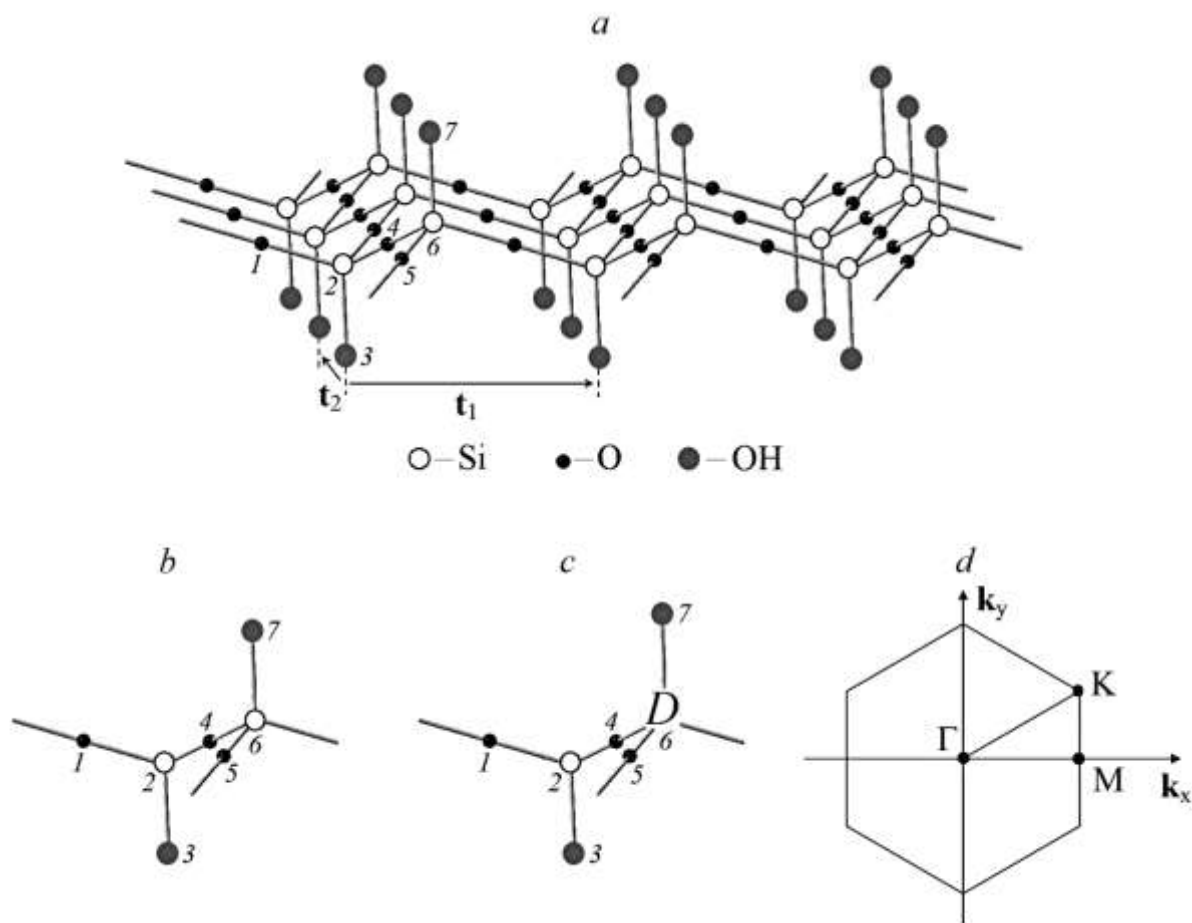


Fig. 1. Single-layer two-dimensional hydroxysiloxane structure: *a* – an elementary cell containing 9 primitive cells, atoms and surface OH groups of one of which are numbered 1-7 (t_1 , t_2 are the basic translation vectors of the primitive cell); *b* - a primitive defect-free cell; *c* - a primitive cell with a defect of substitution of a silicon atom by a D atom; *d* - the Brillouin zone of a two-dimensional hexagonal structure.

Also note that layered structures based on silicon dioxide are the key dielectrics in silicon integrated circuits. Defects in such structures can lead to changes in their electron energy and optical characteristics [4–10]. The features of the electron energy spectrum and optical absorption of single-layer 2D HS structures, both of ideal structure and with substitution defects of surface hydroxide and silanol groups, were studied in [11, 12]. In this paper, we consider the electron energy characteristics of 2D HS structures with defects induced by the isovalent substitution of silicon atoms by titanium and zirconium atoms.

2. Model and details of the calculation scheme

As a two-dimensional unit cell of the 2D HS structure, we chose a structural element containing $N' = 3 \times 3 = 9$ primitive cells of the composition $\text{Si}_2\text{O}_3(\text{OH})_2$ (Fig. 1b). The “defective” structure differs from the “pure” 2D HS structure in that in some primitive cells included in the unit cell, the Si atom is substituted by an isovalent D atom ($D \equiv \text{Ti}, \text{Zr}$) (the corresponding structural formula of a defective primitive cell of composition $\text{SiDO}_3(\text{OH})_2$ is shown in Fig. 1c). The defect concentration will be characterized by the index m , which is equal to the number of primitive cells,

in which substitution took place, per unit cell. Cyclic boundary conditions were imposed on an extended cell consisting $N''=3 \times 3=9$ of elementary cells, each of which includes $N'=3 \times 3=9$ primitive cells (Fig. 1a). This corresponds to the fact that the electron states were calculated taking into account $\tilde{N} = N' \times N''=9 \times 9=81$ the uniformly distributed \mathbf{k} points of the Brillouin zone (Fig. 1d). Symmetrical \mathbf{k} points are represented by their entire star. These points satisfy the relation:

$$\mathbf{k}_{n_1, n_2} = \frac{n_1}{N'} \mathbf{b}_1 + \frac{n_2}{N'} \mathbf{b}_2,$$

where \mathbf{b}_1 and \mathbf{b}_2 are the translation vectors of the reciprocal lattice (they are related to the translation vectors $\mathbf{t}_1, \mathbf{t}_2$ of the primitive cell of the direct lattice (see Fig. 1a) by the condition $(\mathbf{t}_i, \mathbf{b}_j) = 2\pi\delta_{ij}$ ($i, j=1, 2$; δ_{ij} – Kronecker symbol); n_1 and n_2 – integers in the range $[0; N']$. In our case, the translation vectors \mathbf{t}_1 and \mathbf{t}_2 are three times shorter than the translation vectors \mathbf{t}'_1 and \mathbf{t}'_2 of the unit cell. Specific calculations of cyclic models based on an extended cell of large sizes did not lead to a noticeable change in the calculated characteristics. The electron wave functions at intermediate points \mathbf{k} were estimated by interpolation. The grid of numerical integration over spatial coordinates was chosen with such a number of nodes that would ensure the selection in the expansion of the wave function in terms of plane waves of such waves, the energy of which does not exceed 300 Ry [13].

The calculations were performed with complete geometry optimization within the framework of a procedure based on the density functional theory, generalized to objects with translational symmetry (SIESTA software package [14 - 16]), in the valence basis of two-exponential pseudo-orbitals with the inclusion of polarization functions with the same orbital quantum number as valence orbitals (DZP basis). The exchange-correlation potential was chosen as a gradient type in accordance with [17]. The effect of atomic cores was taken into account by introducing the Troullier-Martins-Kleinman-Bylander pseudopotential [18, 19].

The general scheme of the electron energy bands is shown in Fig. 2. The calculated dispersion dependences of the electron energy on the wave vector $\varepsilon(\mathbf{k})$, the density of electron states $\eta(\varepsilon)$ and optical absorption curves (the dependences of the imaginary part of the permittivity ε'' on the energy of absorbed photons $\hbar\omega$) are presented in Fig. 3., and in Fig. 4 – the dependence of various characteristics of the electron energy spectrum on the concentration m of substitution defects.

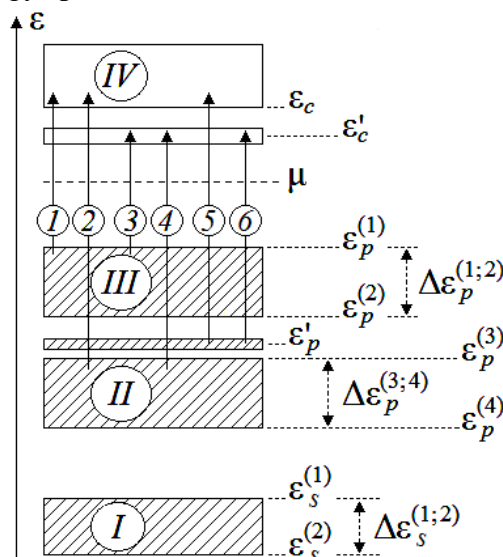


Fig. 2. Scheme of the electron energy spectrum of two-dimensional hydroxysiloxane structures, both defect-free and with substitution defects (arrows 1–6 indicate possible electron transitions; I – valence 2s-band ($\varepsilon_s^{(1)}$ and $\varepsilon_s^{(2)}$ are its upper and lower boundaries, $\Delta\varepsilon_p^{(1;2)}$ is its width); II – low-energy 2p-subband ($\varepsilon_p^{(3)}$ and $\varepsilon_p^{(4)}$ are its upper and lower boundaries, $\Delta\varepsilon_p^{(3;4)}$ is its width); III – high-energy 2p-subband ($\varepsilon_p^{(1)}$ and $\varepsilon_p^{(2)}$ are its upper and lower boundaries, $\Delta\varepsilon_p^{(1;2)}$ is its width); IV – band of vacant states (ε_c is its lower boundary); ε'_p and ε'_c - the subbands of filled and vacant states, respectively, caused by substitution defects; μ - the position of the chemical potential level).

3. Results and discussion

The calculated geometric parameters (bond lengths R and valence angles φ) of the studied 2D HS structures ($R(\text{Si-O}) \approx 1.65 \text{ \AA}$; $R(\text{Ti-OH}) \approx 1.79 \text{ \AA}$; $R(\text{Ti-OSi}) \approx 1.80 \text{ \AA}$; $R(\text{Zr-OH}) \approx 1.91 \text{ \AA}$; $R(\text{Zr-OSi}) \approx 1.94 \text{ \AA}$; $\varphi(\text{OSiO}) \approx 108^\circ\text{--}109^\circ$; $\varphi(\text{OTiO}) \approx 108^\circ\text{--}111^\circ$; $\varphi(\text{OZrO}) \approx 106^\circ\text{--}110^\circ$) are close to the corresponding experimental values of these quantities in both related crystalline and low molecular weight structures [4, 5, 20–23].

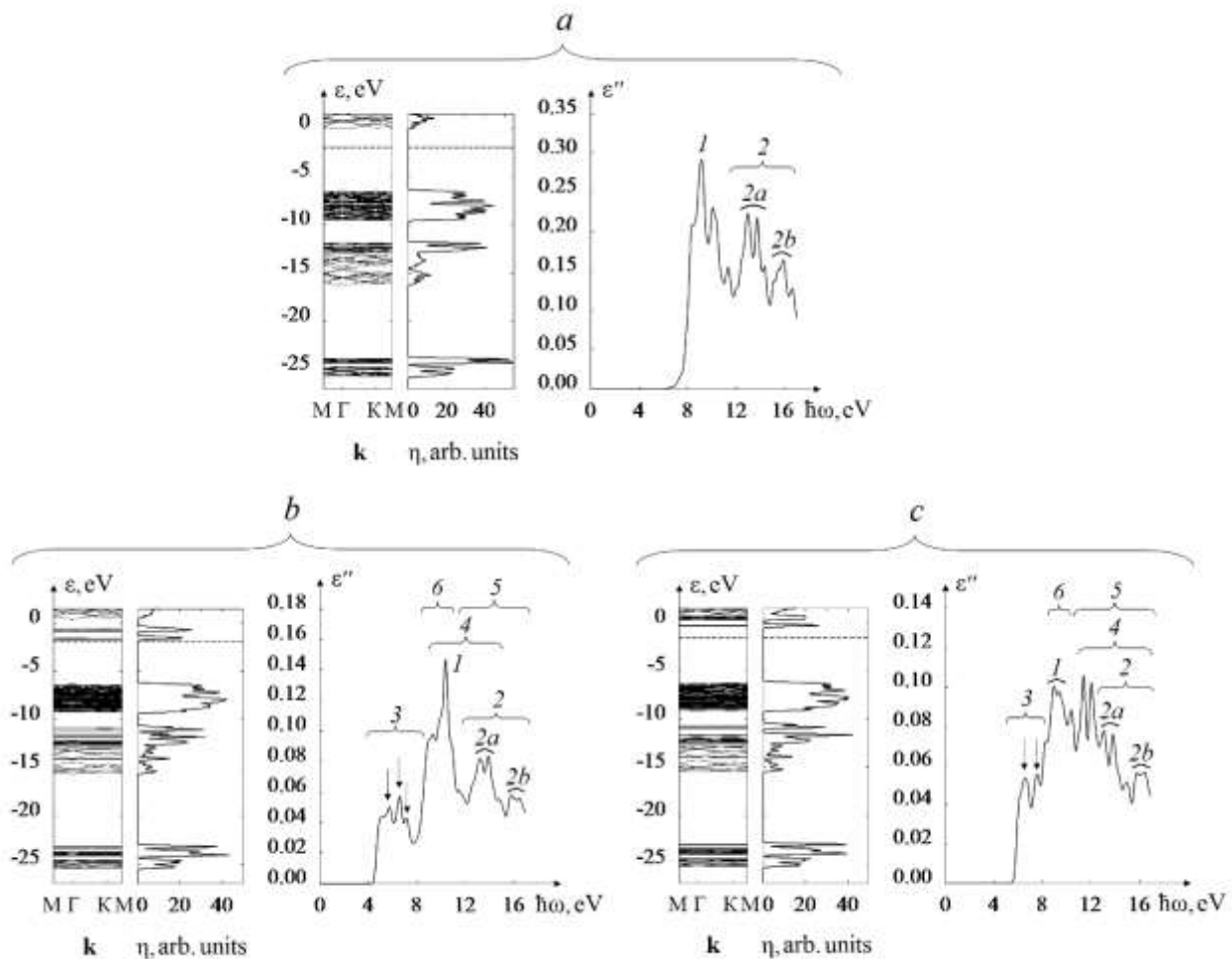


Fig. 3. Dispersion curves $\varepsilon(\mathbf{k})$, densities of one-electron states $\eta(\varepsilon)$, and optical absorption spectra $\varepsilon''(\hbar\omega)$: a – for a defect-free structure ($m = 0$); b –, c – for Ti-, Zr-substituted structures, respectively (for the case $m = 3$). The dotted line marks the position of the chemical potential level μ , the

numbering of the energy regions of absorbed photons is in accordance with the numbering of the transitions in Fig. 2, the arrows mark those bands of the type “3” that do not merge with the bands of type “1” or “6”.

The energy bands (Fig. 2) of 2D HS structures are subdivided into three subbands of occupied states (*I – III*), for which $\varepsilon < \mu$, and a zone (*IV*) of vacant states, for which $\varepsilon > \mu$ (μ – the chemical potential level). The *2s*-valence orbitals of oxygen atoms make the main contribution to the states of the low-energy valence subband (*I*), while the higher-energy valence subbands (*II* and *III*) have the dominant contribution of the *2p*-orbitals of oxygen atoms. The orbitals of silicon and D atoms make the main contribution to the states of the zone of vacant states (*IV*).

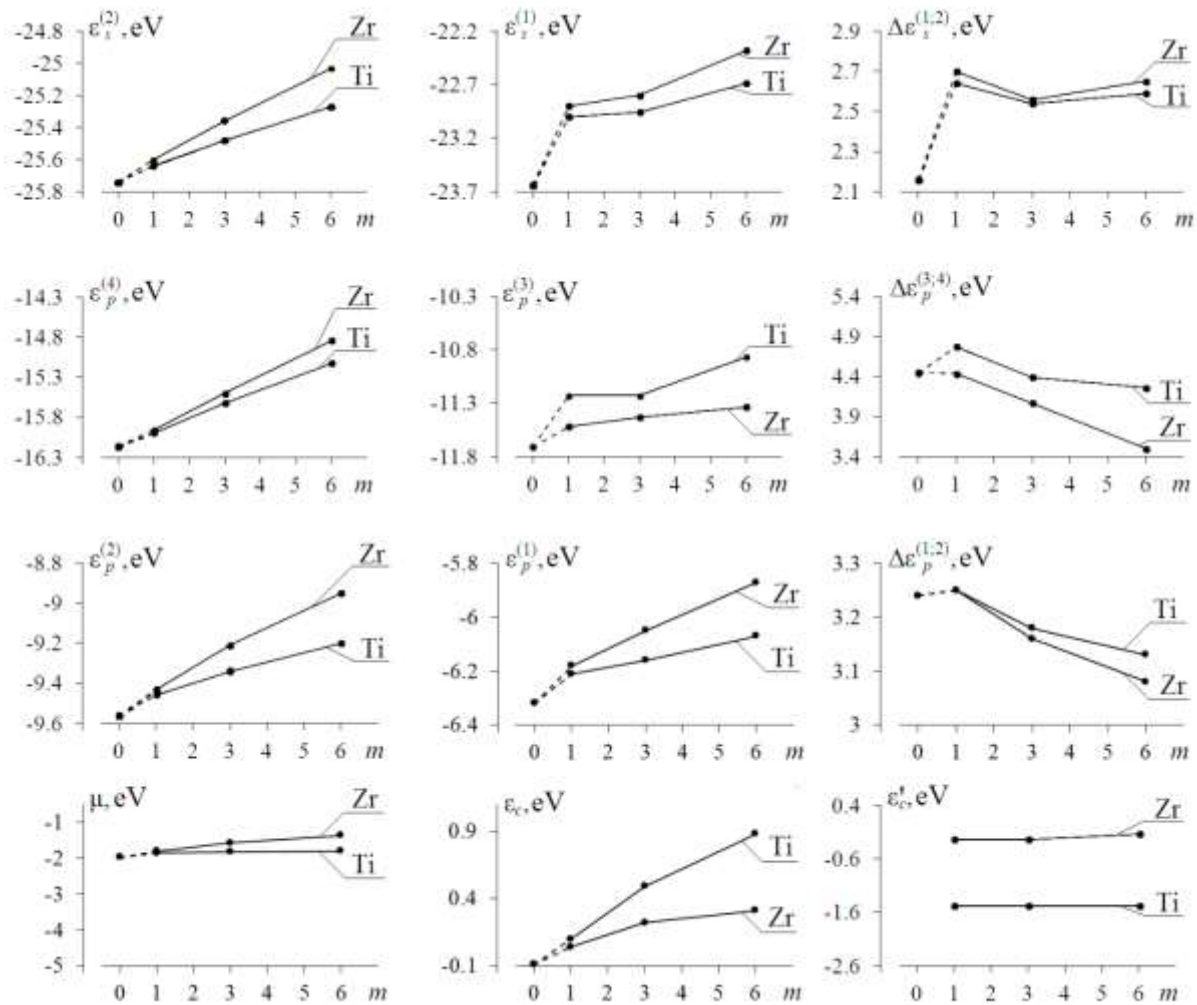


Fig. 4. Dependence of the quantities μ , ε_c , ε'_c , $\varepsilon_s^{(1)}$, $\varepsilon_s^{(2)}$, $\Delta\varepsilon_s^{(1;2)}$, $\varepsilon_p^{(1)}$, $\varepsilon_p^{(2)}$, $\Delta\varepsilon_p^{(1;2)}$, $\varepsilon_p^{(3)}$, $\varepsilon_p^{(4)}$ and $\Delta\varepsilon_p^{(3;4)}$ (notation according to Fig. 2) on the concentration m of defects in the substitution of Si atoms by Ti and Zr atoms ($m = 0$ corresponds to a defect-free structure).

In the defect-free 2D HS structure, the width $\Delta\varepsilon_g$ of the region of forbidden energies ($\Delta\varepsilon_g = \varepsilon_c - \varepsilon_p^{(1)}$; $\varepsilon_p^{(1)}$ and ε_c – the energies corresponding to the upper boundary of the valence band and the lower boundary of the region of vacant states) is ≈ 6.3 eV. This value is included in the

range of band gaps of various modifications of crystalline SiO₂ structures [4, 6, 23-25]. Note that the numerical estimates of $\Delta\varepsilon_g$ may turn out to be underestimated, which is typical for DFT calculations due to “the self-action effects” [26–28] leading to a shift in the energies of vacant states to lower energies. In 2D HS structures with D-substitution, the values of both $\varepsilon_p^{(1)}$ and ε_c are shifted to higher energies: a) at a fixed concentration m of the substitution defect $\varepsilon_p^{(1)}(\text{Si}) < \varepsilon_p^{(1)}(\text{Ti}) < \varepsilon_p^{(1)}(\text{Zr})$; b) for each type of substitutional atoms, with increasing m (from $m = 1$ to $m = 6$), the values $\varepsilon_p^{(1)}$ increase by ≈ 0.15 eV ($D \equiv \text{Ti}$), ≈ 0.3 eV ($D \equiv \text{Zr}$), and the energy ε_c increases by $\approx 0, 3$ eV ($D \equiv \text{Zr}$) and ≈ 0.8 eV ($D \equiv \text{Ti}$).

The energy $\varepsilon_p^{(2)}$ corresponding to the lower boundary of the *III-2p* subband, the electron states of which are determined mainly by the undivided electron pairs of oxygen atoms (in the composition of both siloxane and hydroxide groups), or correspond to weakly bonding orbitals Si(*3p*, *3d*)–O(*2p*) or D(*nd*)–O(*2p*) bonds, with increasing defect concentration m (from $m = 1$ to $m = 6$), monotonically shifts to higher energies by ≈ 0.3 eV ($D \equiv \text{Ti}$), ≈ 0.4 eV ($D \equiv \text{Zr}$), while $\varepsilon_p^{(2)}(\text{Si}) < \varepsilon_p^{(2)}(\text{Ti}) < \varepsilon_p^{(2)}(\text{Zr})$ for all concentrations m . As a result, taking into account the tendency of the energy changes $\varepsilon_p^{(1)}$ (see above), the width $\Delta\varepsilon_p^{(1;2)}$ of the *III-2p* subband either remains almost unchanged (≈ 3.25 eV) at a low degree of substitution ($m = 1$) or slightly decreases (to ≈ 3.1 – 3.2 eV) at growth of m (to $m = 6$).

The energies corresponding to the upper $\varepsilon_p^{(3)}$ and lower $\varepsilon_p^{(4)}$ (Fig. 4) boundaries of the *II-2p* subband, electron states of which are determined by the bonding orbitals of Si–O and D–O bonds, shift to higher energies with increasing defect concentration (this corresponds to weakening of these bonds with oxygen atoms): a) $\varepsilon_p^{(3)}$ increases from ≈ -11.5 eV ($m = 1$; Zr) to ≈ -11.3 eV ($m = 6$; Zr), from ≈ -11.2 eV ($m = 1$; Ti) to ≈ -10.9 eV ($m = 6$; Ti), and at a fixed m $\varepsilon_p^{(3)}(\text{Si}) < \varepsilon_p^{(3)}(\text{Zr}) < \varepsilon_p^{(3)}(\text{Ti})$; b) $\varepsilon_p^{(4)}$ increases from ≈ -16.0 eV ($m = 1$; Ti; Zr) to ≈ -15.1 eV ($m = 6$; Ti) and to ≈ -14.8 eV ($m = 6$; Zr), moreover, at a fixed m $\varepsilon_p^{(4)}(\text{Si}) < \varepsilon_p^{(4)}(\text{Ti}) < \varepsilon_p^{(4)}(\text{Zr})$. As a result of these changes, the width of the *II-2p* subband $\Delta\varepsilon_p^{(3;4)}$ decreases with increasing concentration m : from ≈ 4.8 eV ($m = 1$) to ≈ 4.3 eV ($m = 6$) for $\Delta\varepsilon_p^{(3;4)}(\text{Ti})$ and from ≈ 4.4 eV ($m = 1$) to ≈ 3.5 eV ($m = 6$) for $\Delta\varepsilon_p^{(3;4)}(\text{Zr})$.

The energies corresponding to the upper $\varepsilon_s^{(1)}$ and lower $\varepsilon_s^{(2)}$ (Fig. 4) boundaries of the *I-2s* subband increase for all defect concentrations in the Ti, Zr series, which corresponds to an increase in the bond strengths in the Zr–O, Ti–O series, which was to be expected based on the location of these chemical elements in the periodic system (note that the bond lengths decrease in the same sequence: $R(\text{Zr–O}) > R(\text{Ti–O})$ (see above)). As m increases, $\varepsilon_s^{(1)}$ and $\varepsilon_s^{(2)}$ also shift to higher energies: a) $\varepsilon_s^{(1)}$ increases by ≈ 0.3 eV in the case of Ti substitution and by ≈ 0.5 eV in the case of Zr substitution; b) $\varepsilon_s^{(2)}$ increases by ≈ 0.4 eV in the case of Ti substitution and by ≈ 0.6 eV in the case of Zr substitution. As a result, the width of the *I-2s* subband $\Delta\varepsilon_s^{(1;2)}$ varies within ≈ 2.55 – 2.7 eV with increasing concentration m .

When silicon atoms are substituted by Ti and Zr atoms, the value of μ compared to μ for a defect-free structure is slightly shifted to higher energies by ≈ 0.1 eV ($m = 1$) – 0.2 eV ($m = 6$) (for Ti substitution) and ≈ 0.2 eV ($m = 1$) – 0.6 eV ($m = 6$) (for Zr substitution).

For substituted structures, the impurity states with energy ε'_c split off from the bottom of the conduction band and form narrow bands of vacant states in the band gap of the defect-free structure. These states are mainly due to the $(n-1)d$ orbitals of the substitution atoms.

The degree of penetration of impurity states into the energy gap from the bottom of the conduction band $\delta(\varepsilon'_c) = \frac{\varepsilon_c - \varepsilon'_c}{\Delta\varepsilon_g}$ ($\Delta\varepsilon_g$ refers to a defect-free structure) is characterized by the

following: a) at a fixed substitution concentration m $\delta(\varepsilon'_c; \text{Zr}) < \delta(\varepsilon'_c; \text{Ti})$; b) $\delta(\varepsilon'_c; \text{Zr})$ changes within ≈ 4 – 9% ; $\delta(\varepsilon'_c; \text{Ti})$ – from $\approx 25\%$ to $\approx 38\%$ with increasing m .

Upon isovalent substitution of silicon atoms by atoms of d -elements (Ti, Zr), states with energies ε'_p arise ($\varepsilon_p^{(3)} < \varepsilon'_p < \varepsilon_p^{(2)}$, i.e., corresponding to the energy gap between the $II-2p$ - and $III-2p$ -subbands), due to partially filled d -orbitals of D-atoms. With an increase in the defect concentration, the energies of these states shift to the region of high energies, while they do not go beyond the energy gap (i.e., the condition $\varepsilon'_p < \varepsilon_p^{(2)}$ is not violated).

In this paper, we consider only transitions corresponding to the absorption of photons with energies below 17 eV, i.e., due to electron transitions from the $2p$ -valence subbands. Transitions of electrons from the $I-2s$ -valence subband to the band of vacant states corresponding to the far ultraviolet region were not considered. Analysis of the optical absorption spectra $\varepsilon''(\hbar\omega)$ (Fig. 3) made it possible to establish the following (absorption bands are numbered in Fig. 2).

In the case of a defect-free structure, an absorption bands of type “1” ($III-2p \rightarrow IV$) and two absorption bands of type “2” ($II-2p \rightarrow IV$) appear, corresponding to the energies of absorbed photons $\hbar\omega \approx 9.1$ eV (“1”), 13.4 eV (“2a”) and 15.9 eV (“2b”). Band “2a” has a greater intensity than band “2b”.

For D-substituted structures, with an increase in the degree of substitution m , the transition energies of types “1” and “2” change as follows: a) $\hbar\omega$ (“1”, Ti) increases from ≈ 9.6 eV to ≈ 10.3 eV, $\hbar\omega$ (“1”, Zr) changes in the range of ≈ 9.2 – 9.6 eV; b) $\hbar\omega$ (“2a”, Zr) almost remains at ≈ 13.4 eV, $\hbar\omega$ (“2a”, Ti) increases from ≈ 13.4 eV to ≈ 13.9 eV; c) $\hbar\omega$ (“2b”, Ti) increases from ≈ 15.9 eV to ≈ 16.7 eV, $\hbar\omega$ (“2b”, Zr) varies in the range of ≈ 15.9 – 16.1 eV.

Due to the fact that upon D-substitutions impurity states with energies ε'_c appear in the forbidden region of the defect-free structure between the $III-2p$ subband and the conduction band (see above), bands of type “3” ($III-2p \rightarrow \varepsilon'_c$) and type “4” ($II-2p \rightarrow \varepsilon'_c$) appear in the absorption spectrum. The width $\Delta(\hbar\omega)$ of these bands increases with the growth of m (from $m = 1$ to $m = 6$): a) with Ti-substitution $\Delta(\hbar\omega, \text{“3”}) \approx 4.5$ – 4.9 eV, $\Delta(\hbar\omega, \text{“4”})$ varies within ≈ 5.3 – 6.2 eV; b) with Zr substitution $\Delta(\hbar\omega, \text{“3”}) \approx 3.7$ – 4.8 eV, $\Delta(\hbar\omega, \text{“4”}) \approx 4.7$ – 5.5 eV.

D-substitution also leads to the appearance of bands in the low-energy part of the spectrum caused by transitions of type “3” (Fig. 3). With an increase in the concentration of the substitution defect, the position of these bands shifts to the region of lower energies of absorbed photons, while their intensity increases.

In addition, D-substitution leads to the appearance of states with energies ε'_p ($\varepsilon_p^{(3)} < \varepsilon'_p < \varepsilon_p^{(2)}$) in the energy spectrum, the transitions of electrons involving which to the subband (IV) or to states with energy ε'_c ($\mu < \varepsilon'_c < \varepsilon_c$) cause transitions of type “5” or “6”, respectively, however, these absorption bands are not pronounced, since they overlap with other bands (Fig. 3).

4. Conclusions

Our earlier DFT calculations of bulk and multilayer SiO₂-structures [11, 12], as well as experimental studies by X-ray and photoelectron spectroscopy [24, 29, 30], indicate not only qualitative but also quantitative similarity of the energy schemes of various crystalline modifications of silicon dioxide, which differ in the mutual arrangement of SiO₄-tetrahedra in their structure. The widths of the *II-2p*- and *III-2p*-valence subbands ≈ 5.3 eV and ≈ 3.5 eV obtained by us are in satisfactory agreement with the experimental data [31] (≈ 5.0 eV and ≈ 4.0 eV) and [24, 29] (≈ 5.5 eV and ≈ 5.0 eV). As for the band gap width $\Delta\varepsilon_g$, our DFT calculations lead to values of ≈ 6.0 eV, i.e. underestimated compared to the experimental data (≈ 7.8 – 8.8 eV [24, 25]). The reason for the underestimation of $\Delta\varepsilon_g$ has been discussed above.

For modified 2D HS structures, experimental data on the optical absorption of Ti-substituted SiO₂ films are known [32]. They exhibit an absorption band at $\hbar\omega \approx 5.6$ eV, which is in good agreement with our DFT calculation $\hbar\omega \approx 5.1$ – 5.6 eV (depending on substituent concentration).

The satisfactory agreement between the electron-energy and optical characteristics of the objects studied by us with those experimental data allows us to hope for a sufficient degree of reliability of the results obtained, the most significant of which are as follows.

The isovalent substitution of silicon atoms leads both to a shift in the boundaries of the energy subbands and to a change in their width. In addition, states are generated due to the orbitals of D-atoms, whose energies ε lie in the region of forbidden energies corresponding to a defect-free structure ($\varepsilon_p^{(1)} < \varepsilon < \varepsilon_c$). This is the reason for the appearance of additional bands in the optical absorption spectrum in the region of longer wavelengths (with absorbed photon energies $\hbar\omega \approx 3.2$ – 6.3 eV). This effect is more pronounced with increasing defect concentration.

References

- [1] Tian M, Li M., Li J.C. Effect of size on dielectric constant for low dimension materials. *Physica B Condensed Matter*, 2011, V. 406 (3), 541.
- [2] Shugayev R., Bermel P. Selective absorption and emission on magnetic transitions in low dimensional dielectric structures. *Appl. Phys. Lett.*, 2016, V. 108 (7), 071106.
- [3] Wang H., Liu W., Jin S., Zhang X., Xie Y. Low-Dimensional Semiconductors in Artificial Photosynthesis: An Outlook for the Interactions between Particles/Quasiparticles. *ACS Cent. Sci.*, 2020, V. 6 (7), 1058.
- [4] Büchner C., Heyde M. Two-dimensional silica opens new perspectives. *Progress in Surface Science*, 2017, V. 92 (4), 341.
- [5] Pomp S., Kaden W.E., Sterrer M., Freund H.-J. Exploring Pd adsorption, diffusion, permeation, and nucleation on bilayer SiO₂/Ru as a function of hydroxylation and precursor environment: from UHV to catalyst preparation. *Surf. Sci.*, 2016, V. 652, 286.
- [6] Gao Z., Dong X., Li N., Ren J. Novel Two-Dimensional Silicon Dioxide with in-Plane Negative Poisson's Ratio. *Nano Lett.*, 2017, V. 17(2), 772.
- [7] Guan X., Zhang R., Jia B., Chen X., Yan B., Peng G-D, Li S., Lu P. Electronic and optical properties of Ge-doped silica optical fiber. *Modern Physics Letters B*, 2019, V. 33(12), 1950150.

- [8] Li M., Yang Y., Ling Y., Qiu W., Wang F., Liu T., Song Y., Liu X., Fang P., Tong Y., Li Y. Morphology and doping engineering of Sn-doped hematite nanowire photoanodes. *Nano Letters.*, 2017, V. 17 (4), 2490.
- [9] Yaakob N.H., Wagiran H., Hossain M.I., Ramli A.T., Bradley D.A., Hashim S., Ali H. Thermoluminescence response of Ge- and Al-doped optical fibers subjected to low-dose electron irradiation. *Journal of Nuclear Science and Technology*, 2011, V. 48 (7), 1115.
- [10] Wagiran H., Hossain I., Bradley D.A., Yaakob N.H., Ramli T. Thermoluminescence responses of photon and electron irradiated Ge- and Al-doped SiO₂ optical fibres. *Chinese Physics Letters*, 2012, V. 29 (2), 027802.
- [11] Litinski A.O, Nguyen Thi Sa. Electron energy spectrum and peculiarities of optical absorption in single-layer 2D structures based on silicon dioxide with surface functional groups. *Journal of Surface Investigation. X-ray, Synchrotron and Neutron Techniques*, 2014, V. 8 (3), 549.
- [12] Litinski A.O., Nguyen Thi Sa. Electron energy spectrum of two-dimensional hydroxysiloxane structures with defects of substitution of silanol groups with boron, aluminum, and gallium atoms. *Journal of Surface Investigation. X-ray, Synchrotron and Neutron Techniques*, 2015, V. 9 (6), 1256.
- [13] Moreno J., Soler J.M. Optimal meshes for integrals in real- and reciprocal-space unit cells. *Phys. Rev. B*, 1992, V. 45 (24), 13891.
- [14] Soler J.M., Artacho E., Gale J.D., Garcia A., Junquera J., Ordejon P., Sanchez-Portal D. The SIESTA method for ab initio order-N materials simulation. *J. Phys.: Condens. Matter.*, 2002, V. 14, 2745.
- [15] Artacho E., Anglada E., Dieguez O., Gale J.D., Garcia A., Junquera J., Martin R.M., Ordejon P., Pruneda J.M., Sanchez-Portal D., Soler J.M. The SIESTA method; developments and applicability. *J. Phys.: Condens. Matter.*, 2008, V. 20 (6), 064208.
- [16] Garcia A., Papior N., Akhtar A., Artacho E., Blum V., et al. SIESTA: Recent developments and applications. *Journal of Chemical Physics, American Institute of Physics*, 2020, V. 152 (20), 204108.
- [17] Perdew J.P., Burke K., Ernzerhof M. Generalized Gradient Approximation Made Simple. *Phys. Rev. Lett.*, 1996, V. 77 (18), 3865.
- [18] Troullier N., Martins J.L. Efficient pseudopotentials for plane-wave calculations. *Phys. Rev. B*, 1991, V. 43 (3), 1993.
- [19] Kleinman L., Bylander D.M. Efficacious Form for Model Pseudopotentials. *Phys. Rev. Lett.*, 1982, V. 48 (20), 1425.
- [20] Patnaik P. *Handbook of Inorganic Chemicals*, 1st edition. Publisher: McGraw-Hill Professional; 2002.
- [21] Chibisov A. N. Quantum-mechanical calculations of the Ti and Zr substitution effect on the electronic structure of the nanoporous silicate matrix. *Nanotechnologies in Russia*, 2011, V. 6 (4), 5.
- [22] Gardner M. B. , Westbrook B. R. , Fortenberry R. C. Spectral characterization for small clusters of silicon and oxygen: SiO₂, SiO₃, Si₂O₃, & Si₂O₄. *Planetary and Space Science*, 2020, V. 193, 105076.
- [23] Gao E., Xie B., Xu Z. Two-dimensional silica: Structural, mechanical properties, and strain-induced band gap tuning. *Journal of Applied Physics*, 2016, V. 119 (1), 014301.
- [24] Nekrashevich S.S., Gritsenko V.A. Electronic structure of silicon dioxide (a review). *Physics of the Solid State*, 2014, V. 56(2), 207.
- [25] Xu Y.-N., Ching W.Y. Electronic and optical properties of all polymorphic forms of silicon dioxide. *Phys. Rev. B*, 1991, V. 44 (20), 11048.
- [26] Perdew J.P., Zunger A. Self-interaction correction to density-functional approximations for many-electron systems. *Phys. Rev. B.*, 1981, V. 23(10), 5048.
- [27] Ciofini I., Adamo C., Chermette H. Self-interaction error in density functional theory: a mean-field correction for molecules and large systems. *J. Chem. Phys.*, 2005, V. 123 (1), 67.
- [28] Ciofini I., Adamo C. Effect of self-interaction error in the evaluation of the bond length alternation in trans-polyacetylene using density-functional theory. *J. Chem. Phys*, 2005, V. 123 (12), 121102.
- [29] Gritsenko V.A. Structure of silicon/oxide and nitride/oxide interfaces. *Physics-Uspexhi*, 2009, V. 52 (9), 869.
- [30] DiStefano T.H., Eastman D.E. The band edge of amorphous SiO₂ by photoinjection and photoconductivity measurements. *Sol. State. Commun.*, 1971, V. 9 (24), 2259.
- [31] Shulakov A. S., Braiko A. P., Bukin S. V., Drozd V. E. X-ray spectral analysis of the interface of a thin Al₂O₃ film prepared on silicon by atomic layer deposition. *Physics of the Solid State*, 2004, V.46 (6), 1145.
- [32] Chunxiao Y., Lanfang Y., Linlin T., Xueling F. Effect of Ti doping on microstructure of SiO₂-CTAB mesoporous films. *Journal of Physics: Conference Series*, 2009, V. 188 (1), 012006.